International Journal of Control, Automation, and Systems 21(6) (2023) 1926-1938
http://dx.doi.org/10.1007/s12555-021-0742-4
ISSN:1598-6446 eISSN:2005-4092
http://www.springer.com/12555

# A Sliding Mode Control Scheme for Steering Flexibility and Stability in All-wheel-steering Multi-axle Vehicles

**Tao Xu, Xiangxin Liu, Zheng Li, Bo Feng, Xuewu Ji, and Fuwei Wu***

**Abstract:** Multi-axle vehicles that have important roles in transport systems require high load-carrying capacity, steering performance, and stability. Thanks to the multiple steering characteristics, the dynamic performance of multi-axle vehicles can be greatly improved, which also brings great challenges for the design of their steering controller. Therefore, this paper proposes a steering control scheme for an all-wheel-steering multi-axle vehicle with the goal of optimizing low-speed steering flexibility and high-speed vehicle stability. With the dynamic analyses, the vehicle's steady-state gains at different speeds are reshaped, which provide the closed-loop steering control system with good tracking performance. Correspondingly, a steering controller based on the sliding mode control approach is designed to control the steering angle of each wheel at different axles. The super-twisting control algorithm is also combined with a model-based observer to deal with disturbance while eliminating chattering effects of the control system. Simulation results based on a co-simulation platform verify the efficiency and disturbance rejection of the proposed control approach.

**Keywords:** Multi-axle vehicle, sliding mode control (SMC), steering performance, super twisting control (STC).

## 1. INTRODUCTION

Multi-axle vehicles with large load requirements, such as all-terrain cranes, military vehicles, articulated heavy vehicles, and mining trucks, are often designed with in-wheel motors or independent steering motors to achieve all-wheel drive [1-3] or multi-axle steering [4]. The multi-axle steering mode can directly participate in and affect the vehicle steering process, which is more important than all-wheel drive in improving the vehicle's dynamic performance. Several studies have investigated steering control methods for multi-axle vehicles to improve their maneuverability.

There are multiple steering modes for multi-axle vehicles with independent steering motors, including front- or rear-axle steering, all-wheel steering, diagonal steering, and center steering [5]. Different steering modes have different applications, and all-wheel steering has the broadest adaptability. Correspondingly, its controller design is also complex. Wang *et al.* [6] proposed a proportional control strategy based on the zero side slip angle for a 3-axle-steering vehicle to decrease its steering radius at low speeds and improve the vehicle stability at high speeds. Note that the yaw angle is also a key parameter in the design of all-wheel-steering controllers. Thus, yaw angle was optimized in the design of a steering control system for a 5-axle vehicle based on model predictive control (MPC) to improve the driver's steering efficiency and decrease the vehicle's steering radius in [4]. Moreover, the optimal linear quadratic control algorithm for articulated heavy vehicles with an active semi-trailer steering system was discussed in [7] to improve the roll stability. In [8], a steering controller with two separate proportional-integral-derivative (PID) methods was proposed for a 6WS/6WD vehicle to improve its cornering performance. And in [9], the center of rotation or the steering angles of each wheel was used to design the control strategies for the steering flexibility of multi-axle wheeled robot. Although these studies provide valuable references for the steering control of multi-axle vehicles, how to realize the vehicle steering process like the passenger cars with good steering performance [10] (i.e., steering flexibility at low speeds and stability at high speeds) remains a challenging control issue. Furthermore, the complexity

Manuscript received August 29, 2021; revised December 14, 2021 and March 28, 2022; accepted June 21, 2022. Recommended by Associate Editor Changsun Ahn under the direction of Senior Editor Kyoung Kwan Ahn. This work was supported in part by the Key Laboratory of Transportation Industry of Automotive Transportation Safety Enhancement Technology (Chang'an University) (No. 300102220501); National Natural Science Foundation of China (No. 52104163).

Tao Xu and Xuewu Ji are with the State Key Laboratory of Automotive Safety and Energy, Tsinghua University, Beijing 100084, China (e-mails: ustb_xt@163.com, jixw@mail.tsinghua.edu.cn). Xiangxin Liu, Zheng Li, and Bo Feng are with the Beijing Institute of Space Launch Technology, Beijing 100076, China (e-mails: xiangxin328@126.com, {281886259, 447628890}@qq.com). Fuwei Wu is with the Key Laboratory of Transportation Industry of Automotive Transportation Safety Enhancement Technology, Chang'an University, Xi'an 710064, China (e-mail: wufuwei@chd.edu.cn).
* Corresponding author.

of vehicle systems and uncertain working environments makes controller design for multi-axle vehicles rather difficult. In particular, the disturbance produced by external excitations or model uncertainty can seriously influence vehicular yaw stability at high speeds [11]. Therefore, improving system robustness in the process of effective steering control is another challenge to the design of multi-axle vehicle steering controllers. Yet, these two problems have received little investigation.

In consideration of these two problems above, this paper proposes a control scheme based on the sliding mode control (SMC) method. SMC is a nonlinear control approach that has gained much attention for its capacity to deal with disturbance and uncertainty [12-14]. In existing literatures [15,16], SMC has been widely applied to the steering control of vehicles to enhance the system's robustness. Nevertheless, the traditional SMC strategies described in the above studies have difficulty in dealing with the chattering problem of the control system. Several methods have been used to solve this problem [17,18]. One effective method is the super-twisting control (STC) algorithm [19]. STC is a well-known second-order sliding mode algorithm and has been widely used for system control [20] and observation [21]. According to the author's research, this paper is the first to introduce the SMC and STC approaches into steering controller design for multi-axle vehicles to improve their steering performance.

Referring to the steering control strategies of passenger cars [10,22,23], this paper proposes an optimized steering control scheme for multi-axle vehicles based on the SMC and STC strategies. The main contributions are as follows: 1) The vehicle's steady-state gains at different speeds are reshaped via dynamic analyses to provide good tracking performance for the closed-loop steering control system of a multi-axle vehicle. 2) A steering controller based on the SMC and STC approaches combined with a model-based observer is proposed to control the steering angle of each wheel at different axles to achieve the desired steering performance and deal with disturbances while mitigating the chattering effect of the control system. Finally, a co-simulation platform is implemented to verify the effectiveness and robustness of the proposed control strategies.

The remainder of this paper is organized as follows: Section 2 presents the dynamic model and analyzes the steady-state characteristics for the multi-axle vehicle. In Section 3, a steering controller and disturbance observer are proposed. Section 4 presents the results of simulations of the vehicle under different driving conditions. Conclusions and future research prospects are summarized in Section 5.

## 2. VEHICLE DYNAMIC MODEL

This paper considers a 6-axle vehicle with all-wheel steering to make dynamic analyses and build a dynamic model. In this 6-axle vehicle, the front two axles have a mechanically linked steering system. The steering angle of the two wheels at the second axle is determined by that of the wheels at the first axle, which are all controlled by a driver via the steering wheel. The other wheels at the 3rd, 4th, 5th and 6th axles are steered independently by steering motors.

### 2.1. Dynamic model design

Traditionally, the Ackermann steering approach is often used as the steering theory to reduce tire wear and improve steering control performance. Under the guidance of the Ackermann steering theory, the steering angle of each wheel follows a proportional relationship.

Combined with the above description, a simplified linear dynamic model of this 6-axle vehicle was designed for the steering analyses, as shown in Fig. 1. In this model, $O$ is the mass center; $O$-$x$ is the $x$-coordinate along the longitudinal direction of the vehicle; $O$-$y$ is the $y$-coordinate along the lateral direction of the vehicle; $O_R$ is the steering center of the vehicle; $u$ is the longitudinal velocity while $v$ is the lateral velocity of the vehicle; $\omega$ is the yaw rate of the vehicle around the mass center $O$; $\beta$ is the side slip angle of the vehicle; $l_{io}$ is the longitudinal distance from each axle to the mass center $O$; $i$ represents the $i$th axle; $l_{Ro}$ represents the deflection of steering center that is the longitudinal distance from mass center $O$ to the steering center $O_R$ of the vehicle; $l_{Ro}$ is defined as negative in the left side of mass center $O$ and as positive to the right; $\delta_i$ and $\alpha_i$ are the steering angle and the slid angle of each wheel at $i$th axle, respectively.

In this linear dynamic model, the longitudinal velocity of the vehicle is assumed as constant and the lateral tire force of each wheel is considered to be proportional to its sliding angle. Thus, the linear dynamic model of this 6-axle vehicle can be obtained by

$$\begin{cases} m(\dot{v}+u\omega)=\sum_{i=1}^{6}k_i\left(\delta_i-\beta-\dfrac{l_{io}\omega}{u}\right), \\ I_z\dot{\omega}=\sum_{i=1}^{6}l_{io}k_i\left(\delta_i-\beta-\dfrac{l_{io}\omega}{u}\right), \end{cases} \tag{1}$$

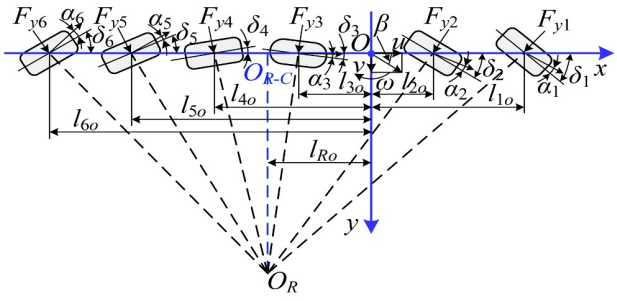


Fig. 1. Schematic of the linear dynamic model of the 6-axle vehicle.

where $m$ is the vehicle mass; $k_i$ is the cornering stiffness of the tire at the $i$th axle; $I_z$ is the moment of inertia of the vehicle.

In this 6-axle vehicle, the Ackermann steering theory determines the relationships between each wheel at different axles. Taking the steering angle of each wheel at the first axle as the reference, the steering angles of the wheels on the other axles can be expressed as

$$\frac{\delta_i}{\delta_1} = \frac{l_{io} - l_{Ro}}{l_{1o} - l_{Ro}} = \varepsilon_i,\ (i = 2,\ ...,\ 6), \tag{2}$$

where $\varepsilon_i$ is the proportionality coefficient. Note that the deflection of steering center $l_{Ro}$ is a particular parameter, which can be used to prove the steering process of the multi-axle vehicle following the Ackermann steering theory.

Define $x_1 = \beta$, $x_2 = \omega$, and $x = [x_1, x_2]$. The linear dynamic model of (1) with consideration of disturbance can be rewritten as

$$\dot{x} = Ax + B\delta_1 + Ed, \tag{3}$$

where

$$A = \begin{bmatrix} a_{11} & a_{12} \\ a_{21} & a_{22} \end{bmatrix} = \begin{bmatrix} -\frac{\sum_{i=1}^{6} k_i}{mu} & -\frac{\sum_{i=1}^{6} k_i l_{io}}{mu^2} - 1 \\ -\frac{\sum_{i=1}^{6} l_{io} k_i}{I_z} & -\frac{\sum_{i=1}^{6} l_{io}^2 k_i}{uI_z} \end{bmatrix},$$

$$B = \begin{bmatrix} b_1 \\ b_2 \end{bmatrix} = \begin{bmatrix} b_{11} + \frac{\sum_{i=2}^{6} b_{1i} l_{io} - \sum_{i=2}^{6} b_{1i} l_{Ro}}{l_{1o} - l_{Ro}} \\ b_{21} + \frac{\sum_{i=2}^{6} b_{2i} l_{io} - \sum_{i=2}^{6} b_{2i} l_{Ro}}{l_{1o} - l_{Ro}} \end{bmatrix},$$

and $b_{1i} = k_i/mu$, $b_{2i} = k_i l_{io}/I_z$, $E = \mathrm{diag}[1, 1]$, and $d = [d_1, d_2]^T$, where $d_1$ and $d_2$ represent the lumped disturbance.

## 2.2. Steady-state steering analysis

Taking the Laplace transform of the linear dynamic model of the vehicle, (3) can be rewritten as

$$\begin{cases} G_\omega(s) = \dfrac{\omega(s)}{\delta_1(s)} = \dfrac{a_{21}b_1 - a_{11}b_2 + b_2 s}{(s - a_{11})(s - a_{22}) - a_{12}a_{21}}, \\ G_\beta(s) = \dfrac{\beta(s)}{\delta_1(s)} = \dfrac{-a_{22}b_1 + a_{12}b_2 + b_1 s}{(s - a_{22})(s - a_{11}) - a_{12}a_{21}}, \end{cases} \tag{4}$$

where $G_\omega(s)$ and $G_\beta(s)$ are the transfer functions. Taking $s = 0$, the steady-state gains in yaw rate and side-slip angle are

$$\begin{cases} G_{\omega(0)} = \dfrac{a_{21}b_1 - a_{11}b_2}{a_{11}a_{22} - a_{12}a_{21}}, \\ G_{\beta(0)} = \dfrac{a_{12}b_2 - a_{22}b_1}{a_{11}a_{22} - a_{12}a_{21}}. \end{cases} \tag{5}$$

For the multi-axle vehicle, it is necessary to improve both flexibility at low speeds and vehicle stability at high speeds. Thus, the desired steady-state gains matter greatly, and can be determined by considering the vehicle's longitudinal speeds. Referring to conventional passenger cars [10,22,23], the value of these two referenced parameters can be modified as

$$\begin{cases} G_{\omega r} = \dfrac{u}{l_r(1 + k_{us}u^2)}, \\ G_{\beta r} = 0, \end{cases} \tag{6}$$

where $G_{\omega r}$ and $G_{\beta r}$ are referenced steady-state gains of yaw rate and side slip angle of the multi-axle vehicle, respectively; $l_r$ is the equivalent wheelbase, and $l_r = l_{1o} + l_{6o}$; $k_{us}$ is the stability factor, and it is a positive constant.

It can be noted that, in accordance with the definition of (6), the referenced steady-state gain in yaw rate changes according to the vehicle speed. There is a large difference from the fixed value of this gain shown in (5). Thus, the performance index term $(G_\omega - G_{\omega r})$ represents a measurement of the vehicle's steerability. In order to make the state of the vehicle steering process tracks the referenced vehicle state, the proportional relationships of the wheel steering angles between the first and other five axles should not be fixed at any vehicle speed. This means that the parameter $l_{Ro}$ should change according to the vehicle speed, which can be expressed by

$$\begin{cases} l_{Rod\_\omega} = \dfrac{\begin{pmatrix} a_{21}\sum_{i=2}^{6} b_{1i}l_{io} - a_{11}\sum_{i=2}^{6} b_{2i}l_{io} \\ -\begin{bmatrix} (a_{11}a_{22} - a_{12}a_{21})G_{\omega r} \\ -a_{21}b_{11} + a_{11}b_{21} \end{bmatrix} l_{1o} \end{pmatrix}}{\begin{pmatrix} -a_{11}\sum_{i=2}^{6} b_{2i} + a_{21}\sum_{i=2}^{6} b_{1i} \\ -\begin{bmatrix} (a_{11}a_{22} - a_{12}a_{21})G_{\omega r} \\ -a_{21}b_{11} + a_{11}b_{21} \end{bmatrix} \end{pmatrix}}, \\ l_{Rod\_\beta} = \dfrac{\begin{pmatrix} (a_{12}b_{21} - a_{22}b_{11})l_{1o} \\ +a_{12}\sum_{i=2}^{6} b_{2i}l_{io} - a_{22}\sum_{i=2}^{6} b_{1i}l_{io} \end{pmatrix}}{\begin{pmatrix} a_{12}b_{21} - a_{22}b_{11} \\ -a_{22}\sum_{i=2}^{6} b_{1i} + a_{12}\sum_{i=2}^{6} b_{2i} \end{pmatrix}}, \end{cases} \tag{7}$$

where $l\_Rod\_\omega$ and $l_{Rod\_\beta}$ are desired deflection of steering center determined by referenced steady-state gains of yaw rate and side slip angle, respectively.

Based on the above analyses, the desired deflection of the steering center $l_{Rod}$ can be calculated with the combination of two parameters $l_{Rod\_\omega}$ and $l_{Rod\_\beta}$, which can be expressed by

$$l_{Rod} = a l_{Rod\_\omega} + b l_{Rod\_\beta}, \tag{8}$$

where $a$ and $b$ are weight coefficients, and $a + b = 1$.

**Remark 1:** By combining (5) and (8), the steady-state gains in yaw rate and side-slip angle are reshaped. They can be used to calculate the desired steering state of the

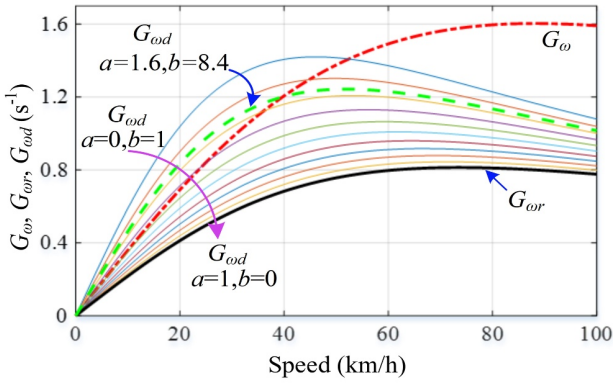


(a)

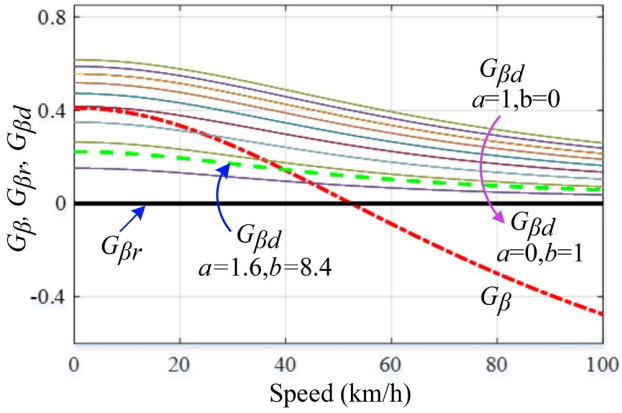


(b)

Fig. 2. Steady-state gains of the multi-axle vehicle: (a) Steady-state gain in yaw rate; (b) Steady-state gain in side-slip angle.

steering controller, which is designed in the following section.

Note that different weight coefficients determine the different desired deflection of the steering center. Accordingly, the desired steady-state gains in yaw rate ($G_{\omega d}$) and side-slip angle ($G_{\beta d}$) will be different, as shown in Fig. 2.

For multi-axle vehicles, low, medium, and high speeds are typically defined as 0-30 km/h, 30-60 km/h, and $>$ 60 km/h, respectively [4]. For the convenience of controller design, we defined low speeds as being $<$40 km/h and high speeds as $>$40 km/h in this paper. Correspondingly, in consideration of the trade-off between low-speed steering flexibility and high-speed vehicle stability, we chose weight coefficients of $a = 1.4$ and $b = 8.6$ to reshape the steady-state gains in yaw rate and side-slip angle, as shown by the green dotted line in Fig. 2.

It can be obtained from Fig. 2, the steady-state gain in yaw rate is significantly improved at low speeds while it is greatly reduced at high speeds. For steady-state gain in side-slip angle, it is greatly improved over the whole speed range. In conclusion, these steady-state gains can satisfy the trade-off between low-speed steering flexibility and high-speed stability for multi-axle vehicle, which can be applied to the tracking performance of the controller design.

## 3. STEERING CONTROLLER DESIGN

### 3.1. Problem description

The objective of the steering controller designed in this paper is to improve the vehicle's steering performance, such as steering flexibility at low speeds, stability at high speeds, and disturbance rejection during the steering process. The main problems in the controller design are as follows:

1) Due to the fixed ratio of the steering angles of the wheels at the first and second axles, the desired steering states at different speeds cannot be achieved, which seriously influences the vehicle steering process. Therefore, it is necessary to design a steering controller that can adjust unreasonable steering processes by controlling the steering angles at the rear four axles.

2) Considering the influence of disturbance on vehicle steering performance, a disturbance observer and compensation controller should be incorporated into the steering controller to improve the robustness of the control system.

With the analyses of steady-state gains in Section 2, the vehicle steering performance can be improved greatly. We simply need to control the real vehicle steering states $\omega_a$ and $\beta_a$ to track the desired values $\omega_d$ and $\beta_d$, which can be calculated with the combination of the vehicle dynamic model (3) and the desired deflection of the steering center described by (8). A flowchart of the complete control strategy is shown in Fig. 3. In this figure, $\theta$ is the steering wheel angle, and $i_\theta$ is the proportionality coefficient between the steering wheel angle and the steering angle of the wheels at the first axle.

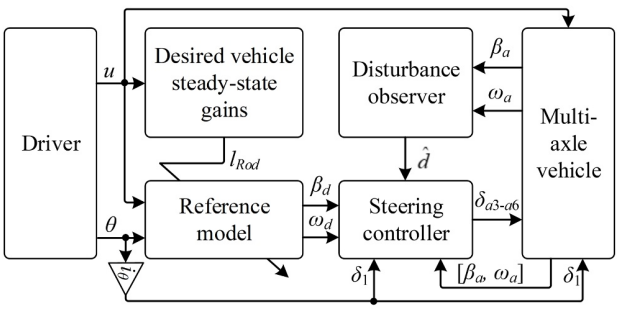


Fig. 3. Flowchart of the steering control system.

### 3.2. Disturbance observer design

As shown in (3), the lumped disturbance has been considered in the vehicle dynamic model. This lumped disturbance represents 'mismatched' disturbances or uncertainties. These are generalized concepts of disturbance that mainly included parameters uncertainties and external disturbance caused by the road or environment. To deal with such disturbance, the following assumptions are required.

**Assumption 1:** The lumped disturbance $d$ and its time derivative are bounded.

**Assumption 2:** The lumped disturbance $d$ and its time derivative have constant values $d_s$ in the steady state.

**Assumption 3:** $(A, B)$ is controllable.

With the assumption above, the lumped disturbance can be estimated by the following theorem.

**Theorem 1** [24]**:** With the description of the dynamic system (3), the disturbance observer can be designed as

$$\begin{cases} \dot{p} = -LE\left(p + Lx_a\right) - L\left(Ax_a + Bu_{in}\right), \\ \hat{d} = p + Lx_a, \end{cases} \tag{9}$$

where $p$ is an instrumental vector; $\widehat{d}$ is the estimated disturbance; $L$ is the observer gain matrix; $u_{in}$ represents the input matrix of the steering angle of each wheel; $X_a$ is actual vehicle state, i.e., $x_a = [x_{a1}, x_{a2}]^T$, $x_{a1} = \beta_a$, $x_{a2} = \omega_a$. Combined with the vehicle dynamic model (3), the actual vehicle dynamic model can be expressed by

$$x_a = Ax_a + B_a u_{in} + Ed, \tag{10}$$

where

$$u_{in} = \begin{bmatrix} \delta_1 & \delta_2 & \delta_{a3} & \delta_{a4} & \delta_{a5} & \delta_{a6} \end{bmatrix},$$
$$B_a = \begin{bmatrix} b_{11} & b_{12} & b_{13} & b_{14} & b_{15} & b_{16} \\ b_{21} & b_{22} & b_{23} & b_{24} & b_{25} & b_{26} \end{bmatrix},$$

where $\delta_{ai}$ $(i = 3, ..., 6)$ are actual inputs of steering angle of wheels at rear four axles.

**Proof:** Defining the error between the real and estimated disturbances

$$e_d = \hat{d} - d \tag{11}$$

Combining (9) and (10), the time derivative of error in (11) can be expressed by

$$\begin{aligned} \dot{e}_d &= \dot{\hat{d}} - \dot{d} \\ &= -LE(p + Lx_a) - L(Ax_a + Bu_{in}) + L\dot{x}_a - \dot{d} \\ &= -LE(p + Lx_a) + LEd - \dot{d} \\ &= -\dot{d} - LE(\hat{d} - d). \end{aligned} \tag{12}$$

Combined with Assumption 2, (12) can be rewritten as

$$\dot{e}_d = -LEe_d. \tag{13}$$

This equation implies that the error $e_d$ equals 0 in a finite time. It can also be verified that the estimated disturbance can track the disturbances asymptotically. The proof is completed. □

### 3.3. Steering controller design

The steering controller is designed to calculate the appropriate steering angles of the wheels at the rear four axles to make the vehicle track the desired state and compensate for disturbance. Namely, it is necessary to appropriately adjust the steering angles of the wheels at the rear four axles under the control of the driver. Therefore, the actual steering inputs can be given as

$$\delta_{ai} = \varepsilon_i \delta_1 + \Delta\delta_{ai}, \tag{14}$$

where $\Delta\delta_{ai}$ are additional angles input used to control the steering process and realize the disturbance rejection for the multi-axle vehicle.

Define the desired vehicle steering state as $x_{1d} = \beta_d$, $x_{2d} = \omega_d$, and $x_d = x_{1d}, x_{2d}] = Ax_d + B\delta_1$. The error between the vehicle's actual and desired state values is defined as

$$e = x_a - x_d. \tag{15}$$

Thus, the time derivative of the vehicle state error can be expressed by

$$\dot{e} = Ae + B_a u_{in} - B\delta_1 + Ed. \tag{16}$$

Combining systems (3) and (10), the error model of (16) can be rewritten as

$$\dot{e} = Ae + B^{\dagger}u^{\dagger} + E\hat{d} + E\tilde{d}, \tag{17}$$

where $\tilde{d}$ is the observation error of disturbance, i.e., $d = \tilde{d} + \hat{d}$, $u^{\dagger}$ is equivalent additional inputs,

$$B^{\dagger} = \begin{bmatrix} b_1^{\dagger} \\ b_2^{\dagger} \end{bmatrix} = \begin{bmatrix} \sum_{i=3}^{6} b_{1i}\varepsilon_i \\ \sum_{i=3}^{6} b_{2i}\varepsilon_i \end{bmatrix}.$$

Combined with the analyses in Section 1, the SMC approach is used in this section. With consideration of disturbance, a combination of two controllers is designed as

$$u^{\dagger} = u_0^{\dagger} + u_s^{\dagger}, \tag{18}$$

where $u_0^{\dagger}$ is nominal controller proposed to yield the desired performance when the system is free from disturbance; $u_s^{\dagger}$ is additional controller that is used to deal with the influence of disturbance.

The integral sliding surface is chosen to design the SMC controller, which is shown as

$$s = G_e\left(e + k_e\int_0^t e dt\right), \tag{19}$$

where $G_e \in \mathbb{R}^{1\times 2}$ is a weight matrix, such that $G_e B^{\dagger} = I_{1\times 1}$. $k_e \in \mathbb{R}^{4\times 4}$ is an appropriately chosen diagonal matrix with positive diagonal elements. The time derivative of $s$ can be given by

$$\dot{s} = \dot{s}_1 + \dot{s}_2$$

$$= \underbrace{\left[G_e(A+k_e)e + u_0^{\dagger} + G_e E\hat{d}\right]}_{\dot{s}_1} + \underbrace{\left[u_s^{\dagger} + G_e E\tilde{d}\right]}_{\dot{s}_2}. \tag{20}$$

To make the system trajectory reach the sliding surface, the equivalent controller $u_0^{\dagger}$ can be defined as (21) by making $s_1 = 0$, which provides a solution to the problem without considering disturbance.

$$u_0^{\dagger} = -G_e(A+k_e)e - G_e E\hat{d}. \tag{21}$$

Thus, (20) can be further rewritten as

$$\dot{s} = \dot{s}_2 = u_s^{\dagger} + \varsigma, \tag{22}$$

where $\varsigma = G_e E\tilde{d}$. In the proposed controller design, the nominal controller ignores the influence of disturbance, which is handled by the additional SMC controller. However, due to the discontinuous nature of the traditional SMC approach, system chattering cannot be avoided [12, 13,19]. Also, discontinuous control input can cause oscillations and actuator abrasions. To remove the chattering effect of the control system, an adaptive STC approach is proposed to address lumped disturbance, which is shown as Theorem 2 below.

**Theorem 2** [12,19,25]**:** Assuming that the time derivative of error disturbance $\varsigma$ in this system is bounded by a constant $d_e$, i.e., $|\dot{\varsigma}| < d_e$, the system's additional controller $u_s$ can be expressed as

$$\begin{cases} u_s = -h_1|s_2|^{1/2}sign(s_2) + \nu, \\ \dot{\nu} = -h_2 sign(s_2), \end{cases} \tag{23}$$

where the gains of $h_1$ and $h_2$ can be properly chosen as

$$\begin{cases} h_1 = h_{c1}\sqrt{\chi} = \kappa\sqrt{\dfrac{2\gamma}{(1-\tau)\alpha}}\sqrt{\chi}, \\ h_2 = h_{c2}\chi = \dfrac{1+\tau}{1-\tau}\chi, \end{cases} \tag{24}$$

where $\chi = k_\chi$, $h_{c1}$ and $h_{c2}$ are two appropriately chosen constants. $\tau$ and $\gamma$ are positive constants, i.e., $0 < \tau < 1$ and $\gamma > 1$; $\kappa$ and $\alpha$ are positive constants that satisfy the inequality

$$\kappa - \frac{2}{\gamma}\alpha > \alpha^2 - \tau(1+\kappa)\alpha + \frac{(1+\kappa)^2}{4}. \tag{25}$$

With the reasonable selection of adaptive gains, $s$ and $\dot{s}_2$ can be converged to 0 asymptotically.

**Proof:** Substituting the additional controller of (23) into (22), one can obtain

$$\begin{cases} \dot{s}_2 = -h_1|s_2|^{\frac{1}{2}}sign(s_2) + \psi, \\ \dot{\psi} = -h_2 sign(s_2) + \dot{\varsigma}, \end{cases} \tag{26}$$

where $\psi = \nu + \varsigma$. A new state vector is designed for the Lyapunov analysis

$$\xi = \begin{bmatrix} \xi_1 \\ \xi_2 \end{bmatrix} = \begin{bmatrix} \chi^{\frac{1}{2}}|s_2|^{\frac{1}{2}}sign(s_2) \\ \psi \end{bmatrix}. \tag{27}$$

The time derivative of this new vector $\xi$ can be written as

$$\dot{\xi} = \frac{\chi}{2|\xi_1|}\begin{bmatrix} -h_{c1} & 1 \\ -2h_{c2} & 0 \end{bmatrix}\xi + \begin{bmatrix} 0 \\ \dot{\varsigma} \end{bmatrix} + \begin{bmatrix} \frac{\dot{\chi}}{2\chi}\xi_1 \\ 0 \end{bmatrix}. \tag{28}$$

With the definition of the new vector $\Lambda = [-h_{c1},\ 1;\ -2h_{c2},\ 0]$, (28) can be rewritten as

$$\dot{\xi} = \frac{\chi}{2|\xi_1|}\Lambda\xi + \begin{bmatrix} 0 \\ \dot{\varsigma} \end{bmatrix} + \begin{bmatrix} \frac{\dot{\chi}}{2\chi}\xi_1 \\ 0 \end{bmatrix}. \tag{29}$$

It is easy to verify that $\Lambda$ is a Hurwitz matrix. Therefore, the Lyapunov function for the proof of the system can be expressed as

$$V = \xi^T P\xi, \tag{30}$$

where $P$ is a constant, symmetric, and positive definite matrix, which can be expressed as

$$P = \frac{1}{2}\begin{bmatrix} 4h_{c2} + h_{c1}^2 & -h_{c1} \\ -h_{c1} & 2 \end{bmatrix}. \tag{31}$$

Furthermore, the time derivative of $V$ is given

$$\dot{V} = \frac{1}{2|\xi_1|}\xi^T(\Lambda^T P + P\Lambda)\xi + q_1\dot{\varsigma}\xi + \frac{\dot{\chi}}{2\chi}\xi_1 q_2\xi, \tag{32}$$

where $q_1 = [-h_{c1},\ 2]$, $q_2 = [4h_{c2} + h_{c1}^2,\ -h_{c1}]$. It is can be known that since $\Lambda$ is a Hurwitz matrix, there exists a positive definite matrix $Q$, such that $\Lambda^T P + P\Lambda = -Q$ and $\lambda_{min}(P)\|\xi\|^2 \le V \le \lambda_{max}(P)\|\xi\|^2$. Therefore, (32) can be rewritten as

$$\dot{V} \le -\frac{\chi}{2}\frac{\lambda_{\min}(Q)}{\lambda_{\max}^{\frac{1}{2}}(P)}V^{\frac{1}{2}} + \frac{d_e\|q_1\|}{\lambda_{\min}^{\frac{1}{2}}(P)}V^{\frac{1}{2}} + \frac{\dot{\chi}}{2\chi}\xi^T\Delta Q\xi, \tag{33}$$

where

$$\Delta Q = \begin{bmatrix} 4h_{c2} + h_{c1}^2 + \frac{h_{c1}}{2} & 0 \\ 0 & \frac{h_{c1}}{2} \end{bmatrix}. \tag{34}$$

Correspondingly, (33) can be presented as

$$\dot{V} \le -\left(\frac{\chi}{2}\frac{\lambda_{\min}(Q)}{\lambda_{\max}^{\frac{1}{2}}(P)} - \frac{d_e\|q_1\|}{\lambda_{\min}^{\frac{1}{2}}(P)}\right)V^{\frac{1}{2}} + \frac{\dot{\chi}}{2\chi}\frac{\lambda_{\max}(\Delta Q)}{\lambda_{\min}(P)}V. \tag{35}$$

For simplicity, three constants are defined as

$$\varpi_1 = \frac{\lambda_{\min}(Q)}{2\lambda_{\max}^{\frac{1}{2}}(P)},\ \varpi_2 = \frac{d_e\|q_1\|}{\lambda_{\min}^{\frac{1}{2}}(P)},\ \varpi_3 = \frac{\lambda_{\max}(\Delta Q)}{2\lambda_{\min}(P)}. \tag{36}$$

Note that $\varpi_1$, $\varpi_2$, and $\varpi_3$ are positive constants. Equation (35) can be further rewritten as

$$\dot{V} \le -(\varpi_1\chi - \varpi_2)V^{\frac{1}{2}} + \varpi_3\frac{\dot{\chi}}{\chi}V. \tag{37}$$

Furthermore, the second time derivative of $V$ can be calculated as

$$\ddot{V} \le \underbrace{-\dot{\chi}V^{\frac{1}{2}} - \varpi_3\frac{\dot{\chi}}{\chi^2}V}_{V_{2-1}} \underbrace{-\frac{(\varpi_1\chi - \varpi_2)\dot{V}}{2V^{\frac{1}{2}}}}_{V_{2-2}} + \underbrace{\varpi_3\frac{\dot{\chi}}{\chi}\dot{V}}_{V_{2-3}}. \tag{38}$$

There are three parts in (38), $V_{2-1}$, $V_{2-2}$, and $V_{2-3}$. It's easy to see that $V_{2-1} < 0$. The size of $\ddot{V}$ dependent on the last two parts $V_{2-2}$, and $V_{2-3}$. Correspondingly, the analyses can be concluded to two cases according to the time derivative of $V$.

1) If $\dot{V} < 0$, Theorem 2 can be proved directly.

2) If $\dot{V} > 0$, it can be concluded that the positive term $V_{2-3}$ will decreases as time goes on. And the term $V_{2-2}$ will become negative from some time instant $t = t_1$, which will dominate the positive term $V_{2-3}$, since $\chi$ is a nondecreasing monotonic function with $\dot{\chi} \ge 0$. Therefore, we can conclude that after the time $t = t_1$, $\ddot{V} < 0$. Therefore, that is to say $V$ is not increasing faster than a time linear function during time $t \in [0, t_1]$, which can be formulated as

$$V \le k_{V1}t + k_{V2}, \tag{39}$$

where $k_{V1}$ and $k_{V2}$ are some positive constants. Then, substituting (39) into (37), we can get

$$\begin{aligned}\dot{V} &\le -(\varpi_1\chi - \varpi_2)V^{\frac{1}{2}} + \varpi_3\dot{\chi}\frac{k_{V1}t + k_{V2}}{k_\chi t + \chi(0)} \\ &\le \underbrace{-(\varpi_1\chi - \varpi_2)V^{\frac{1}{2}}}_{V_{1-1}} + \underbrace{\varpi_3\dot{\chi}\frac{\max\{k_{V1}, k_{V2}\}}{\min\{k_\chi, \chi(0)\}}}_{V_{1-2}},\end{aligned} \tag{40}$$

where $\chi(0)$ is the initial value of $\chi$. Therefore, it can be concluded that after some time $t > t_1$, the first term of (40) that is denoted as $V_{1-1}$ will dominate the second term $V_{1-2}$. Correspondingly, the time derivative of $V$ can be represented as

$$\dot{V} \le -k_{v\theta}(\varpi_1\chi - \varpi_2)V^{\frac{1}{2}}, \tag{41}$$

where $k_{v\theta}$ is equivalent coefficient, i.e., $k_{v\theta} \in (0, 1)$. $\varpi_1\chi - \varpi_2$ has be proved $> 0$ in finite time. Therefore, $s$ and $\dot{s}$ will be converged to zero in finite time. Theorem 2 is proven.□

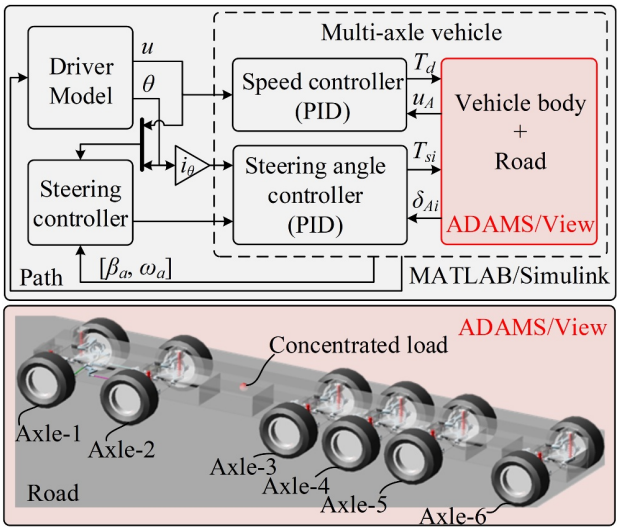


Fig. 4. The block diagram of co-simulation platform.

## 4. CASE STUDY

A 6-axle vehicle was constructed in ADAMS/View, the proposed steering controller was developed in MATLAB/Simulink, and a co-simulation platform based on these two programs was built to verify the analyses and proposed control strategies. ADAMS/View is a professional simulation software package for automatic dynamic analysis of mechanical systems with partial models obtained from real road tests [1,26]. This software uses the Lagrange equation method to establish the system dynamics equation and carry out static, kinematic, and dynamic analyses for multi-body systems. Therefore, it is very suitable for building a simulation model of a multi-axle vehicle with high fidelity and reliability.

In this co-simulation platform, the vehicle model, tire model, and road were built in ADAMS while MATLAB/Simulink was implemented to control the vehicle body and translate the signal between these two software. Its diagram is shown in Fig. 4. In this virtual prototype, $T_d$ is drive torque, which is controlled by speed controller (PID) and used to control the real vehicle speed ($u_A$) with comparison of the desired value ($u$). Similarly, the steering torque $T_{si}$ ($i = 1, ..., 6$ are different axles) controlled by the steering angle controller (PID) are used to control the steering angle ($\delta_{Ai}$) of each wheel of 6-axle vehicle in ADAMS/View. Moreover, a driver model with single-point preview control mode was implemented to control the vehicle to steer with the reference of set path in ADAMS/View [27].

Three driving conditions were implemented to test the steering controller designed in this paper: double-lane changes under 1) low- and 2) high- speed conditions, and 3) straight driving with disturbance. Table 1 presents the vehicle structural parameters used in the simulation.

Table 1. Vehicle structural parameters used in the simulation.

| Parameters | Values | Units |
|---|---|---|
| $m$ | 72000 | kg |
| $I_z$ | 810000 | kg·m$^2$ |
| $l_{1o}$ | 4.5 | m |
| $l_{2o}$ | 2.3 | m |
| $l_{3o}$ | 1.915 | m |
| $l_{4o}$ | 3.565 | m |
| $l_{5o}$ | 5.215 | m |
| $l_{6o}$ | 8.045 | m |
| $k_i$ $(i = 1, ..., 6)$ | 120000 | N/rad |
| $\varepsilon_2$ | 0.712 | - |
| $i_\theta$ | 0.031 | - |

Moreover, in order to verify the effectiveness of proposed control strategy with STC and SMC (denoted as STC-SMC), the control method with traditional SMC (denoted as TSMC) and with linear quadratic regulator (denoted as LQR) were carried out to design the steering controller and compare to the controller with STC-SMC. TSMC is the common method to eliminate the chattering effects of SMC by designing the reaching law ($\dot{s}_2$) with saturation function and boundary layer, as shown in (42). But its control accuracy can be affected while pursuing the smoothness of control inputs, which will be introduced in the case studies as follows:

$$\dot{s}_2 = \begin{cases} -\varepsilon sgn(s_2), & |s_2| > \Delta, \\ -\dfrac{s_2}{\Delta}, & |s_2| \le \Delta, \end{cases} \tag{42}$$

where $\varepsilon$ is the coefficient of saturation, $\Delta$ is the boundary layer thickness.

### 4.1. Double-lane change at low-speed

In this simulation, the vehicle run on a concrete road at a low longitudinal speed ($u = 30$ km/h). Double-lane changes occurred at longitudinal distances of 50 m and 250 m, respectively. The lane width was 5 m and the driving distance was 400 m, as shown in Fig. 5.

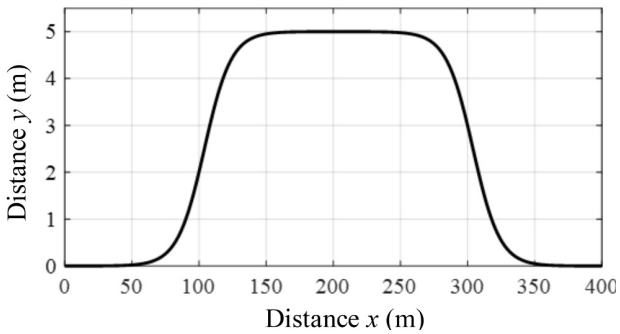


Fig. 5. Lane width for the double-lane change scenario.

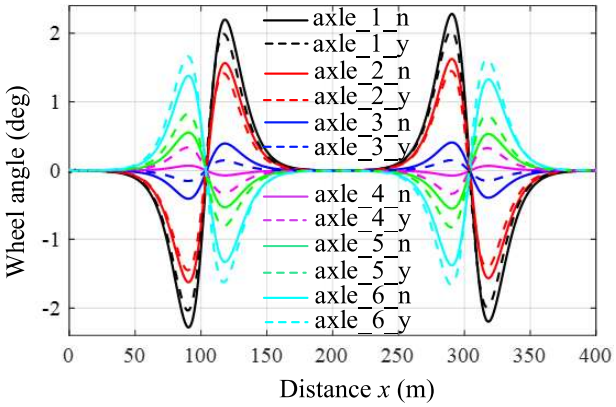


Fig. 6. Simulation results of the steering angles of wheels at different axles under the low-speed condition.

The simulation results of yaw rate and side-slip angle are shown in Fig. 6. In this figure, the simulation results without steering control are denoted as 'Without control', while the simulation results under STC-SMC, TSMC, and LQR control methods are denoted as 'With control (STC-SMC)', 'With control (TSMC)', 'With control (LQR)', respectively. As for the 'Without control', the rear four axles of the vehicle steer under the guidance of the Ackermann steering theory and the control law is calculated by the fixed relationship between the first and second axles. From the results, one can observe that the side-slip angle during steering process with control (STC-SMC, TSMC, or LQR) is significantly lower than that without control. However, the yaw rate increases slightly throughout the steering process. For a comprehensive analysis, these simulation results also need to be combined with the wheel steering angles at different axles (as shown in Fig. 7). In Fig. 7, the simulation results shown as solid lines correspond to the 'Without control' condition in Fig. 6, while the dashed lines represent the results 'With control (STC-SMC)'. By combining Figs. 6 and 7, two conclusions can be obtained: 1) By controlling the steering angles of each wheel at rear four axles, the yaw rate of the vehicle can be increased on the premise of reducing the steering angle of the wheels at the first axle, so as to reduce the driver's steering load and improve steering flexibility. 2) When the wheels at the rear four axles participate in the steering process with control, the vehicle's lateral dynamic performance can be significantly improved, which effectively improves the tracking accuracy of the steering process, as shown in Fig. 8.

Figs. 6 and 8 also shows that the steering controller with STC-SMC, TSMC, or LQR can all make the vehicle steer with better performance at low longitudinal speed. But the steering controller with LQR control method lacks of compensation for the disturbance, and the steering controller with TSMC cannot guarantee both the control accuracy and reducing the chattering effect, which lead to the

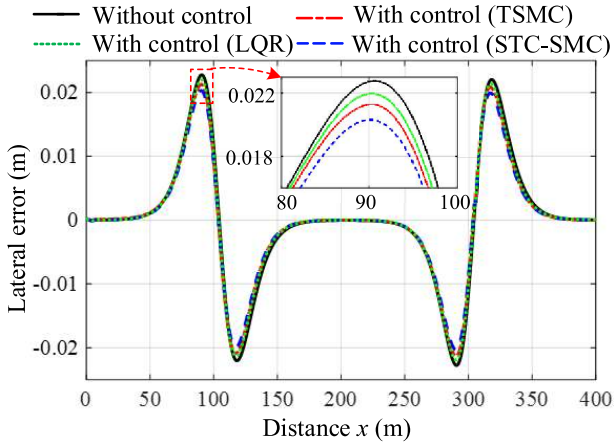


Fig. 7. Simulation results of vehicle lateral tracking error under the low-speed condition.

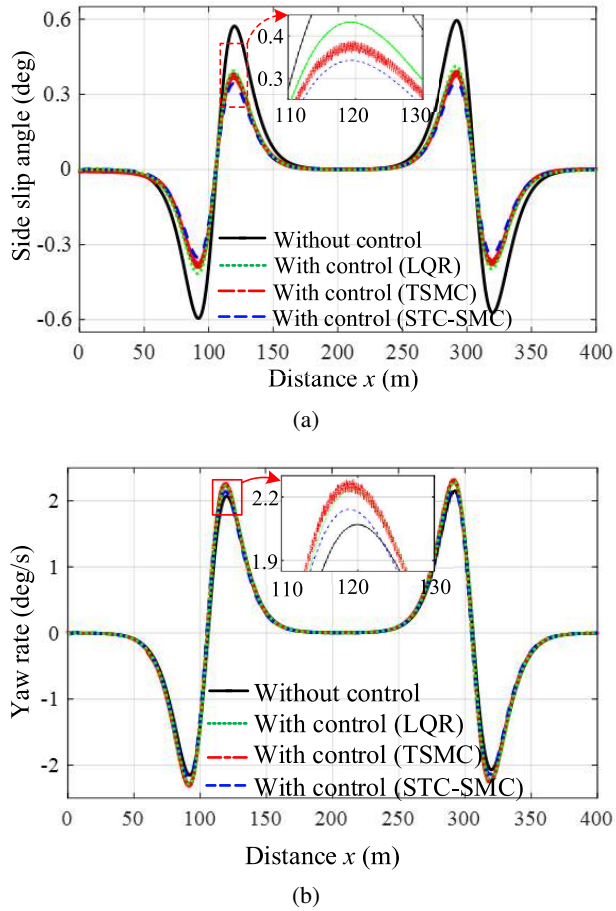


Fig. 8. Simulation results of vehicle states in the double-lane change under the low-speed condition: (a) Side-slip angle; (b) Yaw rate.

unreasonable steering process with higher yaw rate and side-slip angle than the control process with STC-SMC. However, the steering controller with STC-SMC have certain advantage in aspect of dealing with disturbance and eliminating chattering effects, so that the vehicle shows better steering and tracking performance than TSMC and LQR.

Moreover, in order to further evaluate the steering flexibility of the vehicle at low-speed, the steering effort is introduced in this paper, which is defined as shown in the following:

$$Se = \int_0^t |\dot{\theta}|\, dt, \tag{43}$$

where $t$ is the simulation time. Analyzing the steering effort of this 6-axle vehicle at low-speed, the value of $Se$ with control and without control are 75.21 deg and 89.32 deg, respectively. These analyses further verify the effectiveness of the proposed control method in improving the steering flexibility of multi-axle vehicles.

In conclusion, the superior performance described above demonstrates that the steering flexibility and tracking performance of the multi-axle vehicle is greatly improved with STC-SMC control method under low-speed conditions, which is of great benefit to the vehicle's handling and ride comfort.

### 4.2. Double-lane change at high speed

The second simulation verifies the multi-axle vehicle's steering performance under high-speed condition ($u = 100$ km/h). The double-lane changes occurred at longitudinal distances of 50 m and 250 m, respectively. The lane width was 5 m and the driving distance was 500 m.

The simulation results of side-slip angle and yaw rate are shown in Fig. 9. Compared with the steering control objective at low-speed ($u = 30$ km/h), the control objective at high speed is to improve vehicle stability. Fig. 9 clearly shows that the smoother steering process (as evident from the simulation results of side-slip angle and yaw rate) provides better steering performance at high speeds with control (STC-SMC, TSMC, or LQR) than without control. Particularly, the overshoots in yaw rate during steering remain at a very low level, which further illustrates the necessity of the controller design. The simulation results of the steering angles of each wheel at different axles are shown in Fig. 10. By combining Figs. 9 and 10, it can be seen that the driver requires larger steering wheel angle inputs to steer the vehicle in the with control condition. That is also consistent with actual operation requirements, where the operation of the vehicle cannot be too flexible if the driver is to ensure the stability and safety of the vehicle.

Furthermore, the vehicle steering performance with different control methods was compared and analyzed in Figs. 9 and 11. From these simulation results, three conclusions can be obtained: 1) the STC-SMC control method can guarantee both the control accuracy and smoothness of vehicle states with the comparison of the TSMC and

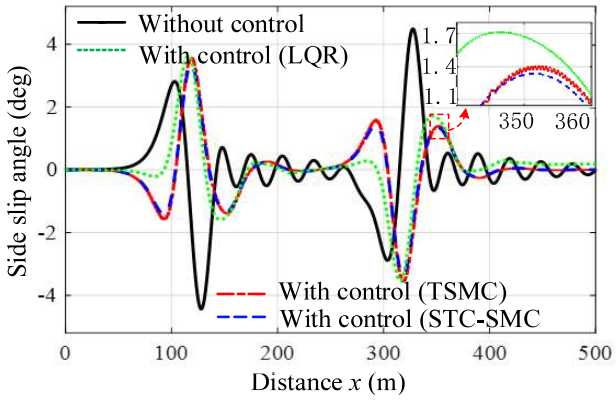


(a)

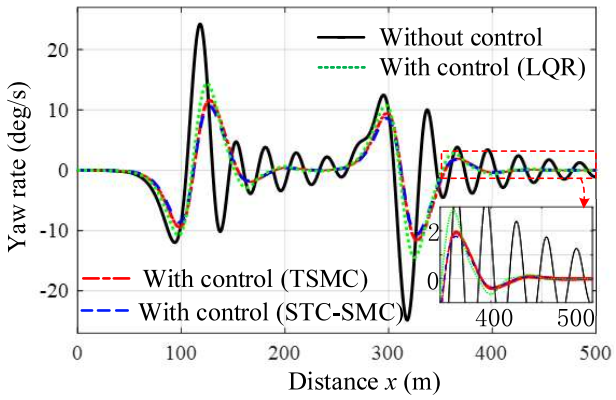


(b)

Fig. 9. Simulation results of vehicle states in the double-lane change at high-speed: (a) Side-slip angle; (b) Yaw rate.

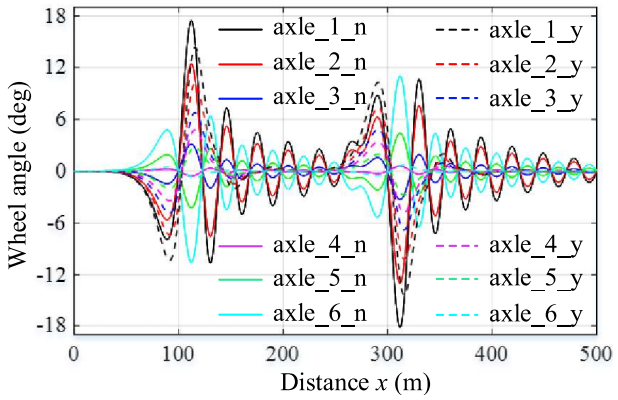


Fig. 10. Simulation results of the steering angles of wheels at different axles under the low-speed condition.

LQR control methods; 2) the maximum lateral error in high-speed steering process with STC-SMC, TSMC and LQR control methods are 0.142 m, 0.158 m, and 0.178 m, respectively, which show a better tracking performance under the proposed control method in this paper; 3) with

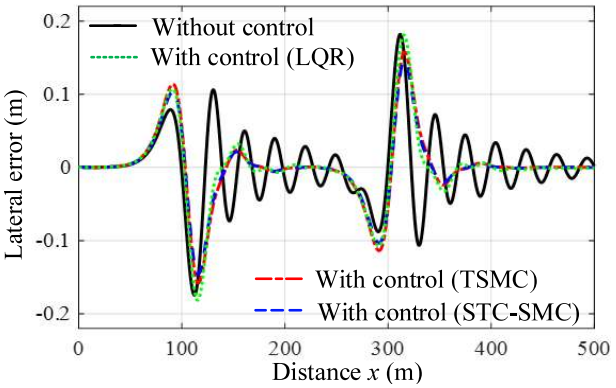


Fig. 11. Simulation results of vehicle lateral tracking error under the high-speed condition.

better vehicle state control (yaw rate and side-slip angle), the vehicle stability can be improved effectively.

In conclusion, the better vehicle states and tracking performance of multi-axle vehicle at high-speed condition shown from these figures demonstrate that the vehicle stability is greatly improved with control. And the proposed STC-SMC control method shows more excellent performance than TSMC and LQR.

### 4.3. Straight-line driving with disturbance

In order to verify the disturbance rejection of the control system, we made the vehicle run in a straight line at high speed ($u = 100$ km/h) and imposed a torque (as disturbance) at the mass center at the longitudinal distance of 50 m. The input disturbance was set as $d = 27.8\sin(\pi t - 0.5\pi)$ kN·m, as shown in Fig. 12.

The simulation results of side-slip angle, yaw rate, and lateral error with different control methods were shown in Fig. 13. From this figure, one can observe that the STC-SMC and LQR control methods can both reduce the influence of disturbance on the vehicle steering process, manifested in the decrease of the oscillation amplitude and pe-

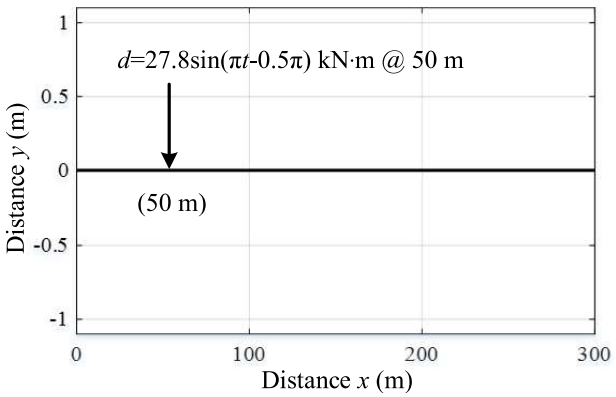


Fig. 12. The referred trajectory and disturbance input.

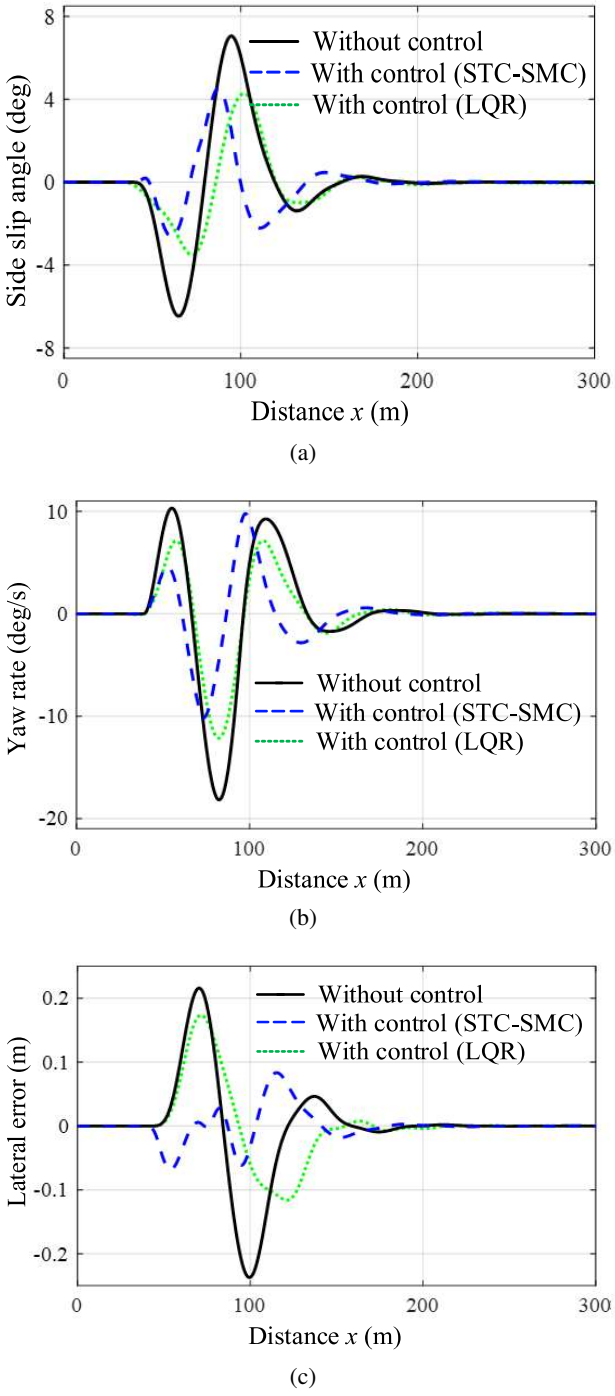


Fig. 13. Simulation results of the vehicle states and tracking error during straight-line driving with a disturbance at 50 m: (a) Side-slip angle; (b) Yaw rate; (c) Lateral error.

riod of the vehicle state. With the comparation of the simulation results without control, the maximum tracking errors of STC-SMC and LQR are reduced by 65% and 18%, respectively. That thanks to the disturbance observer designed for the disturbance compensation of STC-SMC before the disturbance influences the vehicle's motion state, which can be illustrated more clearly by the tracking error in Fig. 13(c).

Based on the overall simulation results, it can be concluded that the proposed steering control scheme can improve the vehicle's steering flexibility and reduce the driver's steering load at low speeds, while vehicle stability is improved greatly at high speeds. At the same time, the control system provides the multi-axle vehicle with more robust performance, which further ensures its stability.

## 5. CONCLUSIONS

This paper investigated an optimized steering controller for a 6-axle vehicle with all-wheel steering. The vehicle steering state is adjusted by controlling the steering angle of each wheel at the rear four axles to achieve low-speed steering flexibility and high-speed vehicle stability. With the dynamic analyses, the vehicle's steady-state gains at different speeds are reshaped, which provides the closed-loop steering control system with good tracking performance. An SMC strategy is adopted to achieve the steering control, while an adaptive STC algorithm and model-based observer are proposed to cope with the disturbance and remove the chattering effect of the control system. A high-fidelity co-simulation model was implemented to verify the efficiency of the controller. The results show that the proposed control strategy can improve vehicular steering performance and has distinct advantages in terms of disturbance rejection.

Though the simulation results were acquired via a co-simulation model, the proposed method still requires real-world testing, which will be done in future work.

## REFERENCES

[1] Y. Shen, Y. Gao, and T Xu, "Multi-axle vehicle dynamics stability control algorithm with all independent drive wheel," *International Journal of Automotive Technology*, vol. 17, no. 5, pp. 795-805, 2016.

[2] Z. Zhang, X. Ma , C. Liu, and S. Wei, "Dual-steering mode based on direct yaw moment control for multi-wheel hub motor driven vehicles: Theoretical design and experimental assessment," *Defence Technology*, vol. 18, no. 1, pp. 49-61, 2022.

[3] M.-A. Ali, C. Kim, S. Kim, A.-M. Khan, J. Iqbal, M.-Z. Khalil, D. Lim, and C. Han, "Lateral acceleration potential field function control for rollover safety of multi-wheel military vehicle with in-wheel-motors," *International Journal of Control, Automation, and Systems*, vol. 15, no. 2, pp. 837-847, 2017.

[4] K. Oh, J. Seo, J.-G. Kim, and K. Yi, "MPC-based approach to optimized steering for minimum turning radius and efficient steering of multi-axle crane," *International Journal of Control, Automation, and Systems*, vol. 15, no. 2, pp. 1799-1813, 2017.

[5] Y. Li, L. Yang, and G. Yang, "Network-based coordinated motion control of large-scale transportation vehicles," *IEEE/ASME Transactions on Mechatronics*, nol. 12, no. 2, pp. 208-215, 2007.

[6] S. Wang, J. Zhang, and H. Li, "Steering performance simulation of three-axle vehicle with multi-axle dynamic steering," *Proc. of IEEE Vehicle Power and Propulsion Conference*, Harbin, 2008.

[7] C. Cheng, and D. Cebon, "Improving roll stability of articulated heavy vehicles using active semi-trailer steering," *Vehicle System Dynamics*, vol. 46, no. 1, pp. 373-388, 2008.

[8] C. Kim, A.-M. Ashfaq, S. Kim, S. Back, and Y. Kim, "Motion Control of a 6WD/6WS wheeled platform with in-wheel motors to improve its maneuverability," *International Journal of Control, Automation, and Systems*, vol. 13, no. 2, pp. 434-442, 2015.

[9] P. Zhang, L. Gao, and Y. Zhu, "Study on control schemes of flexible steering system of a multi-axle all-wheel-steering robot," *Advances in Mechanical Engineering*, vol. 8, no. 6, pp. 1-13, 2016.

[10] E. Esmailzadeh, A. Goodarzi, and G. -R. Vossoughi, "Optimal yaw moment control law for improved vehicle handling," *Mechatronics*, vol. 13, no. 7, pp. 659-675, 2003.

[11] K. Kim, B. Kim, Y. Go, J. Park, J. Park, I. S, and K. Yi, "An investigation on motor-driven power steering-based cross-wind disturbance compensation for the reduction of driver steering effort," *Vehicle System Dynamics*, vol. 52, no. 7, pp. 922-947, 2014.

[12] Y. Zheng, J. Liu, X. Liu, D. Fang, and L. Wu, "Adaptive second-order sliding mode control design for a class of nonlinear systems with unknown input," *Mathematical Problems in Engineering*, vol. 2015, Article ID 319495, 2015.

[13] C. Hu, R. Wang, F. Yan, Y. Huang, H. Wang, and C. Wei, "Differential steering based yaw stabilization using ISMC for independently actuated electric vehicles," *IEEE Transactions on Intelligent Transportation Systems*, vol. 19, no. 2, pp. 627-638, 2018.

[14] M. Zhang, Y. Zhang, and X. Cheng, "An enhanced coupling PD with sliding mode control method for underactuated double-pendulum overhead crane systems, " *International Journal of Control, Automation, and Systems*, vol. 17, no. 6, pp. 1579-1588, 2019.

[15] C. -L. Hwang, C. -C. Yang, and J. -Y. Hung, "Path tracking of an autonomous ground vehicle with different payloads by hierarchical improved fuzzy dynamic sliding-mode control," *IEEE Transactions on Fuzzy Systems*, vol. 26, no. 2, pp. 899-914, 2017.

[16] E. Mousavinejad, Q.-L. Han, F. Yang, Y. Zhu, and L. Vlacic, "Integrated control of ground vehicles dynamics via advanced terminal sliding mode control," *Vehicle System Dynamics*, vol. 55, no. 2, pp. 268-294, 2016.

[17] J. A. Burton and A. S. I. Zinober, "Continuous approximation of variable structure control," *International Journal of Systems Science,* vol. 17, no. 6, pp. 875-885, 1986.

[18] J. Yang, S. Li, and X. Yu, "Sliding-mode control for systems with mismatched uncertainties via a disturbance observer," *IEEE Transactions on Industrial Electronics*, vol. 60, no. 1, pp. 160-169, 2013.

[19] J. A. Moreno and M. Osorio, "Strict Lyapunov functions for the super-twisting algorithm," *IEEE Transactions on Automatic Control*, vol. 57, no. 4, pp. 1035-1040, 2012.

[20] S. P. Sadala and B. M. Patre, "A new continuous sliding mode control approach with actuator saturation for control of 2-DOF helicopter system," *ISA Transactions*, vol. 74, pp. 165-174, 2018.

[21] J. Davila, L. Fridman, and A. Levant, "Second-order sliding-mode observer for mechanical systems," *IEEE Transactions on Automatic Control*, vol. 50, no. 11, pp. 1785-1789, 2005.

[22] R. Tchamna and I. Youn, "Yaw rate and side-slip control considering vehicle longitudinal dynamics," *International Journal of Automotive Technology*, vol. 14, no.1, pp. 53-60, 2013.

[23] Q. Lu, A. Sorniotti, P. Gruber, J. Theunissen, and J. De Smet, "H∞ loop shaping for the torque-vectoring control of electric vehicles: Theoretical design and experimental assessment," *Mechatronics*, vol. 35, pp. 32-43, 2016.

[24] J. Yang, A. Zolotas, W. H. Chen, K. Michail, and S. Li, "Robust control of nonlinear MAGLEV suspension system with mismatched uncertainties via DOBC approach," *ISA Transactions*, vol. 50, no. 3, pp. 389-96, 2011.

[25] A. Chalanga, S. Kamal, and B. Bandyopadhyay, "A new algorithm for continuous sliding mode control with implementation to industrial emulator setup," *IEEE/ASME Transactions on Mechatronics*, vol. 20, no. 5, pp. 2194-2204, 2015.

[26] Y. Wang, and C. Wang, "Matching and optimising analysis of multi-axle steering vehicle steering system," *International Journal of Vehicle Design*, vol. 76, no. 1, pp. 82-109, 2018.

[27] Y. Liu, X. Ji, K. Yang, X. He, X. Na, and Y. Liu, "Finite-time optimized robust control with adaptive state estimation algorithm for autonomous heavy vehicle," *Mechanical Systems and Signal Processing*, vol. 139, 106616, 2020.

**Tao Xu** is currently a Post-doctoral of Vehicle Engineering with the Tsinghua University. He received his Ph.D. degree in mechanical engineering from University of Science and Technology Beijing, China in 2019 and his B.S. degree in vehicle engineering from Shandong University of Science and Technology, Shandong Provence of China in 2013. His research interests include articulated heavy vehicle design and control, and vehicle dynamics and control.

**Xiangxin Liu** received his M.S. degree in aerospace propulsion theory and engineering from Beihang University in 2002, and a B.S. degree from Jiangsu Institute of Petrochemical Technology in 1997. He is currently with Beijing Institute of Space Launch Technology, Beijing, China. His research interests include aerospace ground equipment design, vehicle system design, and finite element analysis.

**Zheng Li** received his M.S. degree in armament science and technology from China Academy of Launch Vehicle Technology in 2022, and a B.S. degree from Harbin Institute of Technology in 2019. He is currently with Beijing Institute of Space Launch Technology, Beijing, China. His research interests include aerospace ground equipment design, vehicle system design, and vehicle dynamic control.

**Bo Feng** received his B.S. degree in vehicle engineering from the School of Automotive Engineering, Wuhan University of Technology in 2007. His research interests include technological innovation and application of new energy vehicles, and reliability and redundancy verification of wire control technology.

**Xuewu Ji** received his B.S., M.S., and Ph.D. degrees in automotive engineering from the College of Automotive Engineering, Jilin University, China, in 1987, 1990 and 1994, respectively. He is currently an Associate Professor at State Key Laboratory of Automotive Safety and Energy, Tsinghua University, China. His research interests include vehicle dynamics and control, and advanced steering system technology. Dr. Ji received the National Science and Technology Progress Award for his achievements in the industrialization of electric power steering technology in 2014.

**Fuwei Wu** received his B.S. degree in traffic safety engineering, and his M.S. and Ph.D. degrees in vehicle operation engineering from Chang'an University, Xi'an, China, in 2009, 2012, and 2020, respectively. He was an Engineer with the School of Automobile, Chang'an University, where he is now a Senior Engineer. His research interests include driver behavior analysis, pedestrian behavior analysis, and traffic safety engineering.